J Mater Sci: Mater Electron (2015) 26:4862–4869
DOI 10.1007/s10854-015-2994-3

Microstructures and microwave dielectric properties of $(1 - x)Sr_{0.2}Na_{0.4}Sm_{0.4}TiO_3$–$xLnAlO_3$ (Ln = Nd, Pr and Sm) ceramic systems

Jingjing Qu[1] · Changlai Yuan[2] · Fei Liu[2,3] · Xinyu Liu[2,3] · Guohua Chen[2] · Panpan Qin[2]

Received: 12 January 2015 / Accepted: 23 March 2015 / Published online: 29 March 2015

Abstract The microstructures and microwave dielectric properties of the $(1 - x)Sr_{0.2}Na_{0.4}Sm_{0.4}TiO_3$–$xLnAlO_3$ samples (where Ln stands for Nd, Pr and Sm, $x = 0.2$–0.3) were studied. The XRD result showed that the $(1 - x)Sr_{0.2}Na_{0.4}Sm_{0.4}TiO_3$–$xLnAlO_3$ (Ln = Nd, Pr and Sm) solid-solutions with single orthorhombic perovskite phase could be formed in the componential range of $0.2 \leq x \leq 0.3$. With an increasing of Ln^{3+} content, the dielectric constant (ε_r) decreased due to the smaller dielectric polarizability of $LnAlO_3$ than that of $Sr_{0.2}Na_{0.4}Sm_{0.4}TiO_3$. With increasing x from 0.2 to 0.3, the quality factor ($Q{\cdot}f$) firstly increased and then decreased for the specimens with $PrAlO_3$, because the $Q{\cdot}f$ values were strongly depended on grain sizes. Moreover, either increasing the A-site bond valence or decreasing the B-site bond valence led to a decrease in the temperature coefficient of the resonant frequency (τ_f). Typical values of $\varepsilon_r \sim 52.7$, $Q{\cdot}f \sim 9700$ GHz (at 4.33 GHz) and $\tau_f \sim 1.5$ ppm/°C were obtained for the $(1 - x)Sr_{0.2}Na_{0.4}Sm_{0.4}TiO_3$–$x SmAlO_3$ ($x = 0.25$) ceramic sintered at 1470 °C for 4 h.

✉ Fei Liu
liufeiguet@163.com

[1] Department of Information Engineering, Guilin University of Aerospace Technology, Guilin 541004, People's Republic of China

[2] College of Material Science and Engineering, Guilin University of Electronic Technology, Guilin 541004, People's Republic of China

[3] College of Material Science and Engineering, Central South University, Changsha 410083, People's Republic of China

1 Introduction

With the rapid development of the mobile and satellite communication, microwave electronic devices are required to be developed and fabricated for miniaturization and integration. Materials with the perovskite structure are widely employed as these microwave electronic devices. Furthermore, perovskites materials are characterised by the chemical formula ABO_3, and a structure which is very tolerant to substitution for ions of various sizes on both A- and B-site cation sublattices [1, 2]. In order to fulfill the materials with a high dielectric constant (ε_r), a moderate quality factor ($Q{\cdot}f$) and a near zero temperature coefficient of resonant frequency (τ_f), two compounds, one with $SrTiO_3$-based or $CaTiO_3$-based [3–6] materials and the other with those materials of negative τ_f values [7–14], have been mixed to form a solid solution or composite.

In our previous work, the Sr^{2+} substitutions for $(Ca_{0.61}Nd_{0.26})^{2+}$ and $(Ca_{0.4}Sm_{0.4})^{2+}$ could form a solid solution in $(1 - x)SrTiO_3$–$xCa_{0.61}Nd_{0.26}TiO_3$ [15] and $(1 - x)SrTiO_3$–$xCa_{0.4}Sm_{0.4}TiO_3$ [16] ceramics, respectively. These $SrTiO_3$-based materials were similar with the most of interesting $CaTiO_3$-based materials [17–23] for microwave communication and passive component applications. In the present work, similarly, the $Sr_{1-x}Na_{x/2}Sm_{x/2}TiO_3$ ceramics (Abbreviation as SNSTx) could also from a solid solution in the componential range of $0.7 \leq x \leq 0.9$. The preferable microwave dielectric properties with $\tau_f \sim 297$ ppm/°C, $\varepsilon_r \sim 125$ and $Q{\cdot}f \sim 3500$ GHz (at 2.76 GHz) were obtained for the SNSTx ($x = 0.8$) samples sintered at 1350 °C for 4 h, which was briefly analysed below. Moreover, the high positive τ_f of the SNST0.8 ceramics could be suppressed to small or zero τ_f by addition of a high negative τ_f microwave ceramics, which made it a suitable candidate for microwave applications. It was reported that $LnAlO_3$ (Ln = La, Pr, Nd,

Sm Dy, Y and Er) materials had low dielectric loss and a high negative τ_f [9, 10, 24, 25]. The SNST0.8 and $LnAlO_3$ (Ln = Nd, Pr and Sm) ceramics belonged to a same or distorted perovskite structure. Thus, the microstructures and microwave dielectric properties of the $(1-x)(Sr_{0.2}Na_{0.4}Sm_{0.4})TiO_3$–$xLnAlO_3$ (Ln = Nd, Pr and Sm, $0.2 \leq x \leq 0.3$) ceramic systems were researched in the present work (referred to hereafter as SNST-NAx, SNST-PAx and SNST-SAx).

2 Experimental

The $(1-x)Sr_{0.2}Na_{0.4}Sm_{0.4}TiO_3$–$xLnAlO_3$ (Ln = Nd, Pr and Sm, $x = 0.2, 0.25, 0.3$) specimens were prepared by the conventional solid state reaction method. The starting materials are Nd_2O_3, Pr_6O_{11}, Sm_2O_3, $SrCO_3$, Na_2CO_3, Al_2O_3 and TiO_2 powders with high-purity reagent-grade (more than 99.9 %). These powders are mixed according to the desired compositions and ground in distilled water for 24 h with ZrO_2 balls. The mixtures are dried and calcined at 1200 °C for 2 h. The calcined powders mixed with an appropriate amount of PVA (5 wt%) as a binder were ground and sieved through 100-mesh screen, then pressed into pellets with 10–11 mm in diameter and 4.5–5.0 mm in thickness. All samples were prepared using an automatic uniaxial hydraulic press at 150 MPa. These pellets were preheated at 650 °C for 2 h to expel the binder, then sintered at 1400–1520 °C for 4 h in air.

Ceramic densification was assessed from mass and dimension measurements. Structural analysis was undertaken by X-ray diffraction (XRD) using a Brukerd8-advance system. Microstructures were examined by scanning electron microscopy (SEM) (JSM-5610LV). The dielectric behaviors at microwave frequency of the samples were measured by the $TE_{01\delta}$ shielded cavity method [26] using a network analyzer and a temperature chamber (Agilent E5230C). The quality factor was characterized by $Q{\cdot}f$ (Q = 1/dielectric loss, f = resonant frequency) value at 2.5–4.7 GHz. The τ_f value was calculated by the following formula [27]:

$$\tau f = \frac{\Delta f_0}{f_0 \Delta T} = \frac{f_{75} - f_{25}}{f_{25} \times 50} \quad (1)$$

where f_{75} and f_{25} represent the resonant frequencies at 75 and 25 °C, respectively.

3 Results and discussions

3.1 $Sr_{1-x}Na_{x/2}Sm_{x/2}TiO_3$ ceramics

Figure 1a shows the typical XRD patterns of the SNST0.9, SNST0.8 and SNST0.7 ceramics sintered at 1350 °C for 4 h. It can be seen that the solid solution based on pure orthorhombic perovskite phase, belonging to the space group Pnma(62), is identified for all samples. The similar results have also been confirmed in the (Sr, Ca, Ln)TiO_3 (Ln = Nd and Sm) ceramics [15, 16]. Moreover, all diffraction peaks of the orthorhombic phase slightly shift to the smaller angles with increasing Sr^{2+} content due to the substitution of larger Sr^{2+} (1.44 Å, CN = 12) for $(Sm_{1/2}Na_{1/2})^{2+}$ (1.37 Å, CN = 12) at A-site ion [28]. Figure 1b shows the magnified (121) peak shifting to the lower angles, which accords with the Vegard's law. The surface morphologies of SNST0.9, SNST0.8 and SNST0.7 ceramics sintered at 1350 °C for 4 h are detected by SEM, as shown in Fig. 1c–e, respectively. It can be observed that the surfaces of the sintered samples exhibit a dense grain structure, and very small grains of 1–3 μm are observed at Fig. 1c, then the average grain sizes increase with increasing Sr^{2+} content (see Fig. 1d, e).

The microwave dielectric properties (ε_r, $Q{\cdot}f$ value and τ_f value) of the SNSTx ceramics sintered at 1350 °C/4 h as a function of x are shown in Fig. 2. The dielectric constant (ε_r) decreases continually from 143 to 108 and the τ_f values shift observably from 433.7 to 127.1 ppm/°C with the decrease in Sr^{2+} content. It indicates that the ε_r and τ_f value are sensitive to the Sr/(Sm, Na) ratio in the SNSTx ($0.7 \leq x \leq 0.9$) ceramics. Similar result was also confirmed in our previous work [15, 16]. For the quality factor ($Q{\cdot}f$) of the SNSTx ceramics, the maximum [~3500 GHz (at 2.76 GHz)] is obtained at $x = 0.8$. It seems likely that the low $Q{\cdot}f$ values of ceramics are mostly due to the large number of grain boundaries existed in the SNST0.9 sample and the abnormal large grains detected at the SNST0.7 sample (see Fig. 1c, e). These phenomenons can affect the dielectric loss of ceramics [29, 30]. The initial goal of our studies is to find a new dielectric material for microwave application. Consequently, the SNST0.8 ceramics with $\tau_f \sim 297$ ppm/°C, $\varepsilon_r \sim 125$ and $Q{\cdot}f \sim 3500$ GHz (at 2.76 GHz) are selected to combine with $LnAlO_3$ (Ln = Nd, Pr and Sm) ceramics for a detailed investigation below.

3.2 $(1-x)Sr_{0.2}Na_{0.4}Sm_{0.4}TiO_3$–$xLnAlO_3$ ceramics

The XRD patterns of the SNST-NAx, SNST-PAx and SNST-SAx ($0.2 \leq x \leq 0.3$) ceramics sintered at 1470 °C for 4 h are shown in Fig. 3a–c, respectively. For all specimens, a single phase with orthorhombic perovskite, belonging to the space group Pnma (62), is obtained in the range of $0.2 \leq x \leq 0.3$. These results are similar with that of the pure SNSTx ($0.7 \leq x \leq 0.9$) specimens, as shown in Fig. 1a. In addition, the insets of Fig. 3a–c show a magnified (121) peak. This suggests that the (121) peak slightly shift to a higher angle with increasing $LnAlO_3$ content due to the incorporation of the smaller Al^{3+} (0.535 Å) in place

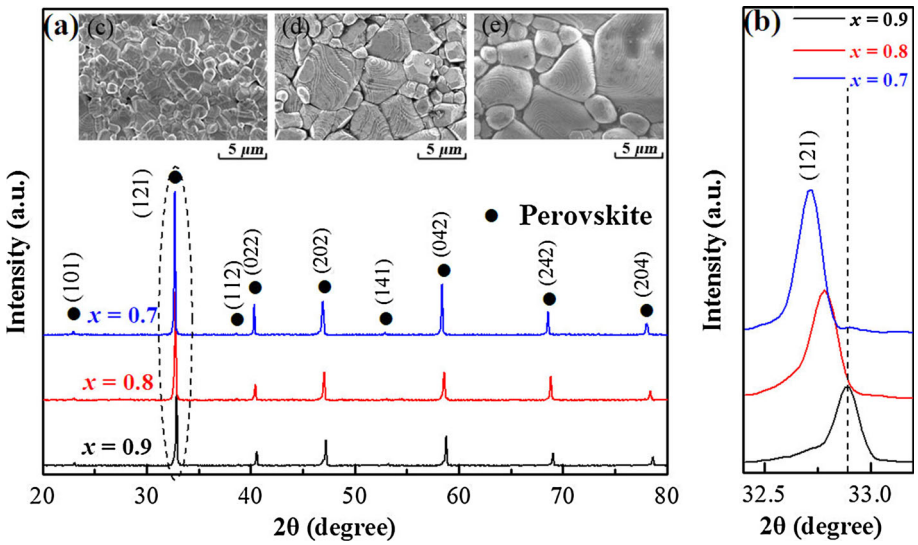

Fig. 1 **a** X-ray diffraction patterns of the SNSTx ($0.7 \leq x \leq 0.9$) ceramics sintered at 1350 °C/4 h. **b** The magnified (121) peak. The *insets* show SEM surface morphologies of **c** SNST0.9, **d** SNST0.8 and **e** SNST0.7 samples sintered at 1350 °C/4 h, respectively

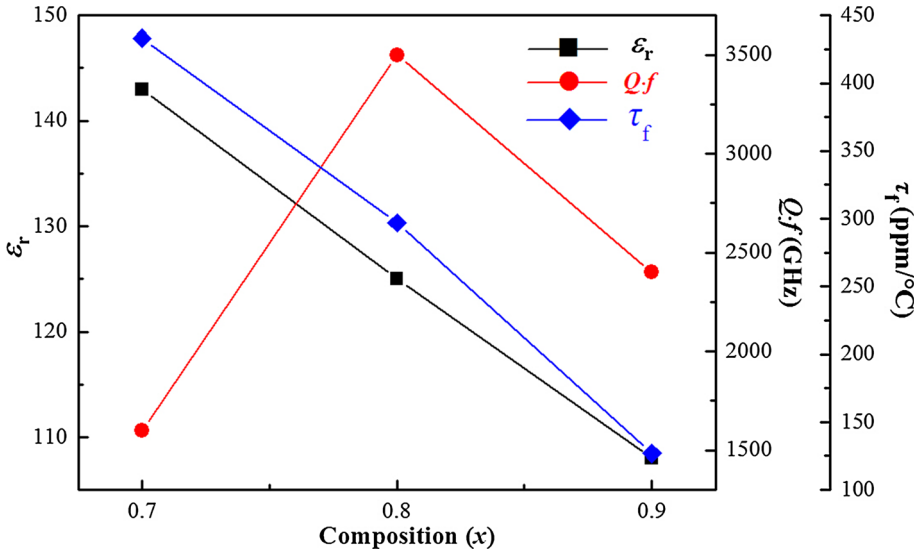

Fig. 2 Microwave dielectric properties (ε_r, $Q{\cdot}f$ value and τ_f value) of the SNSTx ($0.7 \leq x \leq 0.9$) ceramics sintered at 1350 °C/4 h

of Ti^{4+} (0.605 Å) for B-site ion and the partly substitution of smaller Ln^{3+} (Nd = 1.27 Å, Pr = 1.17 Å and Sm = 1.24 Å) for $(Sr_{0.2}Na_{0.4}Sm_{0.4})^{2+}$ (1.38 Å) at A-site ion [28]. The lattice parameters and unit cell volumes of the SNST-NAx, SNST-PAx and SNST-SAx ceramics are calculated from the XRD patterns and the results are illustrated in Table 1. It can be seen that the unit cell volume gradually decreases with an increase in $LnAlO_3$ content (Ln = Nd, Pr and Sm), respectively. This phenomenon obeys the general known Vegard's law as well.

Typical grain microstructural photographs of the SNST-NAx, SNST-PAx and SNST-SAx ($0.2 \leq x \leq 0.25$) ceramics sintered at 1470 °C for 4 h are shown in Fig. 4. The average grain sizes of the SNST-NAx ($x = 0.2$, 0.25) specimens are small compared with that of the specimen with $x = 0.3$, and a small number of imperfect grain boundaries are observed in Fig. 4a1–a3. In addition, the SNST-PAx ($x = 0.2$, 0.25) specimens exhibit very small grains of 2–4 μm and very big grains over 10 μm, as shown in Fig. 4b1, b2. And it is clear that the abnormal larger grains exceeded 35 μm are observed for the SNST-PAx ($x = 0.3$) specimens in Fig. 4b3. Moreover, a well-developed and uniform microstructure can be achieved at the SNST-SA0.2 specimens (see Fig. 4c1). Also the average grain size slowly increases and no obvious pores are shown in microscopic surface of the SNST-SA0.25 and SNST-SA0.3 specimens, as illustrated in Fig. 4c2, c3, respectively.

Figure 5a1–a3 show the relative densities of the SNST-NAx, SNST-PAx and SNST-SAx ($0.2 \leq x \leq 0.3$) ceramics at different sintering temperatures for 4 h, respectively. For all samples, the densities initially increase with increasing

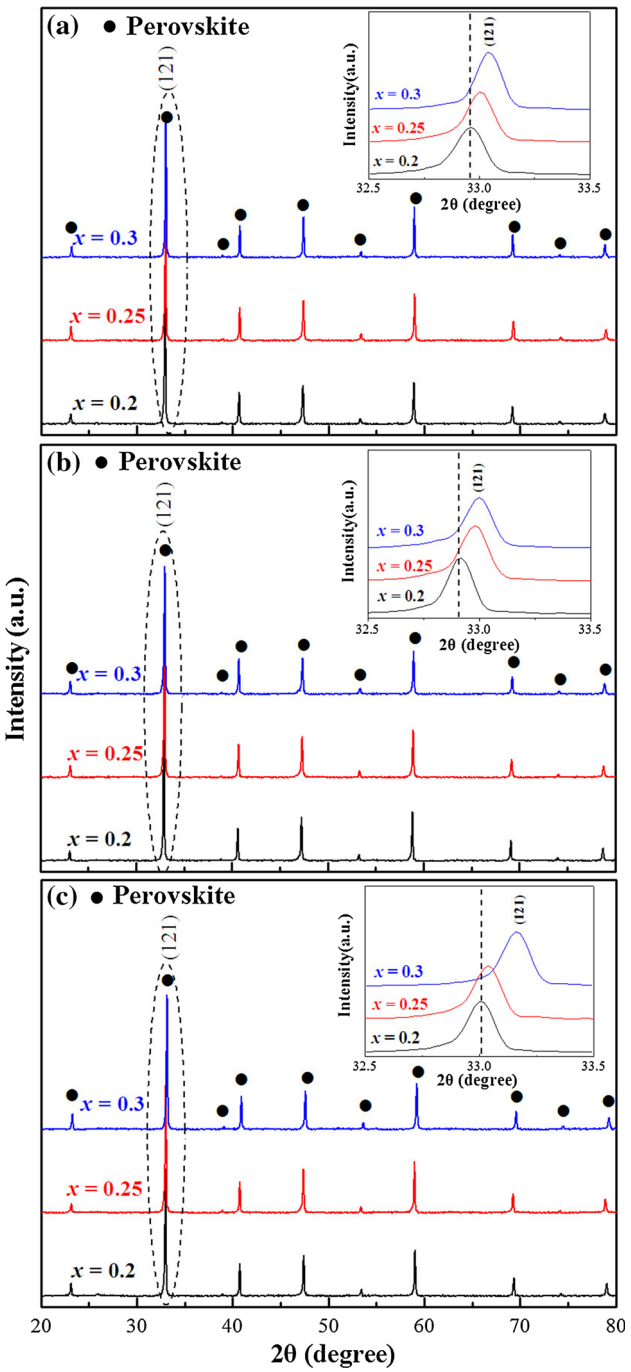

Fig. 3 X-ray diffraction patterns of the **a** SNST-NAx, **b** SNST-PAx and **c** SNST-SAx ($0.2 \leq x \leq 0.3$) specimens sintered at 1470 °C/4 h. The *inset* shows a magnified (121) peak

sintering temperature and reach a maximum, then slightly decrease at a higher sintering temperature. The changes of dielectric constant (ε_r) for the SNST-NAx, SNST-PAx and SNST-SAx ($0.2 \leq x \leq 0.3$) ceramics as functions of various sintering temperatures are demonstrated in Fig. 5b1–b3, respectively. The ε_r of all the samples increases to a maximum value in a certain sintering temperature, corresponding to the optimum densification temperature. According to the graphs, the variation of ε_r with sintering temperatures is generally consistent with the change trend of the relative densities at the same x, which also confirms that the ε_r is significantly dependent upon the compactness. On the other hand, the ε_r decreases with the increase of $LnAlO_3$ (Ln = Sm, Nd) content due to the smaller dielectric polarizability of $NdAlO_3$ (11.83 Å^3), $PrAlO_3$ (12.14 Å^3) and $SmAlO_3$ (11.56 Å^3) than that of $(Sr_{0.2}Na_{0.4}Sm_{0.4})TiO_3$ (12.51 Å^3) [31]. Also, as seen in Fig. 5b1–b3, the ε_r in the specimens with $PrAlO_3$ is slightly higher than that of the specimens with $NdAlO_3$ and $SmAlO_3$. It can be explained by the larger ionic polarizability of Pr^{3+} (5.32 Å^3) than that of Nd^{3+} (5.01 Å^3) and Sm^{3+}(4.74 Å^3) [31]. Moreover, a maximum ε_r value ~63.7 is obtained for the SNST-PA0.2 specimen sintered at 1450 °C for 4 h. Therefore, in addition to the relative density, the variance in the dielectric constant (ε_r) can be attributed to the change of dielectric and ionic polarizability.

The room-temperature $Q{\cdot}f$ values of the SNST-NAx, SNST-PAx and SNST-SAx ($0.2 \leq x \leq 0.3$) ceramics sintered at different temperatures for 4 h are demonstrated in Fig. 6. It is observed that the $Q{\cdot}f$ values of all the specimens are insensitive to the sintering temperatures with an increasing of $LnAlO_3$ content due to the fact that the relative densities of all the specimens are higher than 96 % and the compactness of ceramics is closely related with the sintering temperature. In addition, the effects of secondary phase on the $Q{\cdot}f$ value have been neglected because the secondary phase has not been detected, as illustrated in Fig. 3. Consequently, we infer that the $Q{\cdot}f$ value is strongly dependent on grain sizes and grain boundaries in these ceramics systems. The $Q{\cdot}f$ value of the SNST-NAx and SNST-SAx specimens increases with the rise of x, as shown in Fig. 6a, c, respectively. However, in Fig. 6b, the $Q{\cdot}f$ value increases firstly with x up to 0.25 and then decreases for the SNST-PAx specimens. This is due to the large irregular grains existing in the SNST-PA0.3 specimen (see Fig. 4b3). Based on the classical damped oscillator model, the $Q{\cdot}f$ value is inversely proportional to the dielectric constant (ε_r) in the infrared frequency range. For the SNST-PAx ($0.2 \leq x \leq 0.3$) specimens, the variation of $Q{\cdot}f$ value is not consistent with that of ε_r. These results obviously break the mentioned rule and can be attributed to influences from external factors, which also confirms that the $Q{\cdot}f$ values of these ceramics systems are largely depended on grain sizes and grain boundaries. Similar results in the $(1-x)(Ca_{0.7}Nd_{0.2})TiO_3$–$x(Li_{0.5}Nd_{0.5})TiO_3$ ceramics are also reported by Kim et al. [32]. Furthermore, it can be perceived that the optimal $Q{\cdot}f$ value (~9700 GHz) is obtained in the SNST-SA0.25 specimen sintered at 1470 °C for 4 h, the reason can be related to the more uniform grain size and the less imperfect grain boundaries in the SNST-SA0.25 specimen.

Table 1 Lattice parameters and cell volume of the SNST-NAx, SNST-PAx and SNST-SAx ($0.2 \leq x \leq 0.3$) ceramics sintered at 1470 °C/4 h

Ln	x	a (Å)	b (Å)	c (Å)	$\alpha = \beta = \gamma$ (°)	Unit cell volume (Å3)
Nd	0.2	5.4285	7.6683	5.4205	90	225.64
	0.25	5.4244	7.6631	5.4152	90	225.10
	0.3	5.4205	7.6563	5.4155	90	224.75
Pr	0.2	5.4303	7.6892	5.4348	90	226.93
	0.25	5.4251	7.6706	5.4303	90	225.98
	0.3	5.4250	7.6632	5.4209	90	225.30
Sm	0.2	5.4206	7.6622	5.4186	90	225.06
	0.25	5.4197	7.6534	5.4132	90	224.54
	0.3	5.4189	7.6688	5.3885	90	223.93

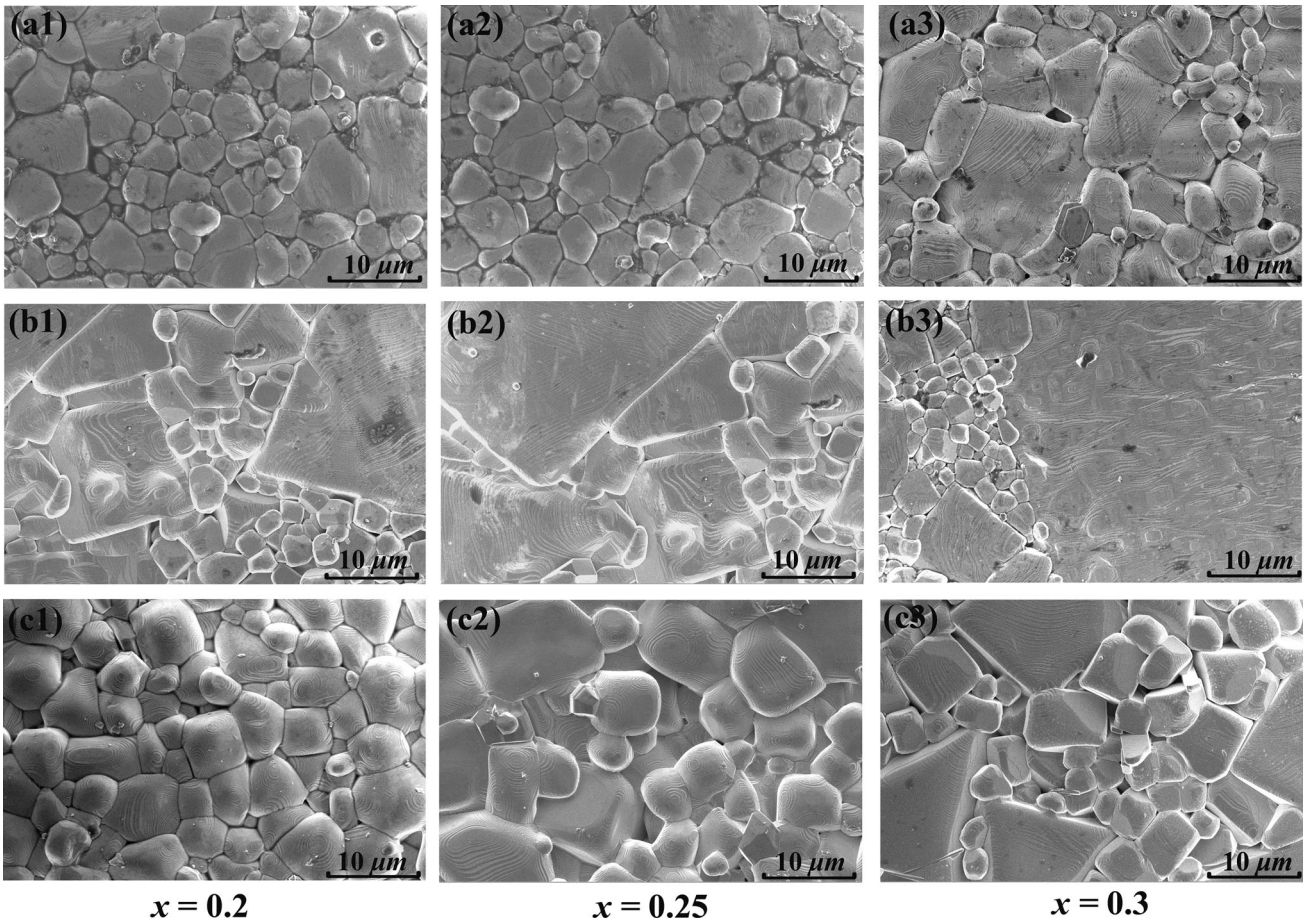

Fig. 4 SEM micrographs of the **a1–a3** SNST-NAx, **b1–b3** SNST-PAx and **c1–c3** SNST-SAx ($0.2 \leq x \leq 0.3$) ceramics sintered at 1470 °C for 4 h

Replacing $(Sr_{0.2}Na_{0.4}Sm_{0.4})^{2+}$ and Ti^{4+} with Ln^{3+} and Al^{3+} in the $(1-x)Sr_{0.2}Na_{0.4}Sm_{0.4}TiO_3$–$xLnAlO_3$ (Ln = Nd, Pr and Sm, $0.2 \leq x \leq 0.3$) ceramics leads to the variation in atomic interactions, which results in a change of bond valence for the materials. The bond valence of the SNST-NAx, SNST-PAx and SNST-SAx ceramics is calculated using the following equations [33]:

$$V_i = \sum v_{ij} \tag{2}$$

$$v_{ij} = \exp\left[\frac{R_{ij} - d_{ij}}{b}\right] \tag{3}$$

where R_{ij} is the bond valence parameter, d_{ij} is the length of a bond between atom i and j, and b is a universal constant (0.37 Å) [33]. The results are recorded in Table 2. With an

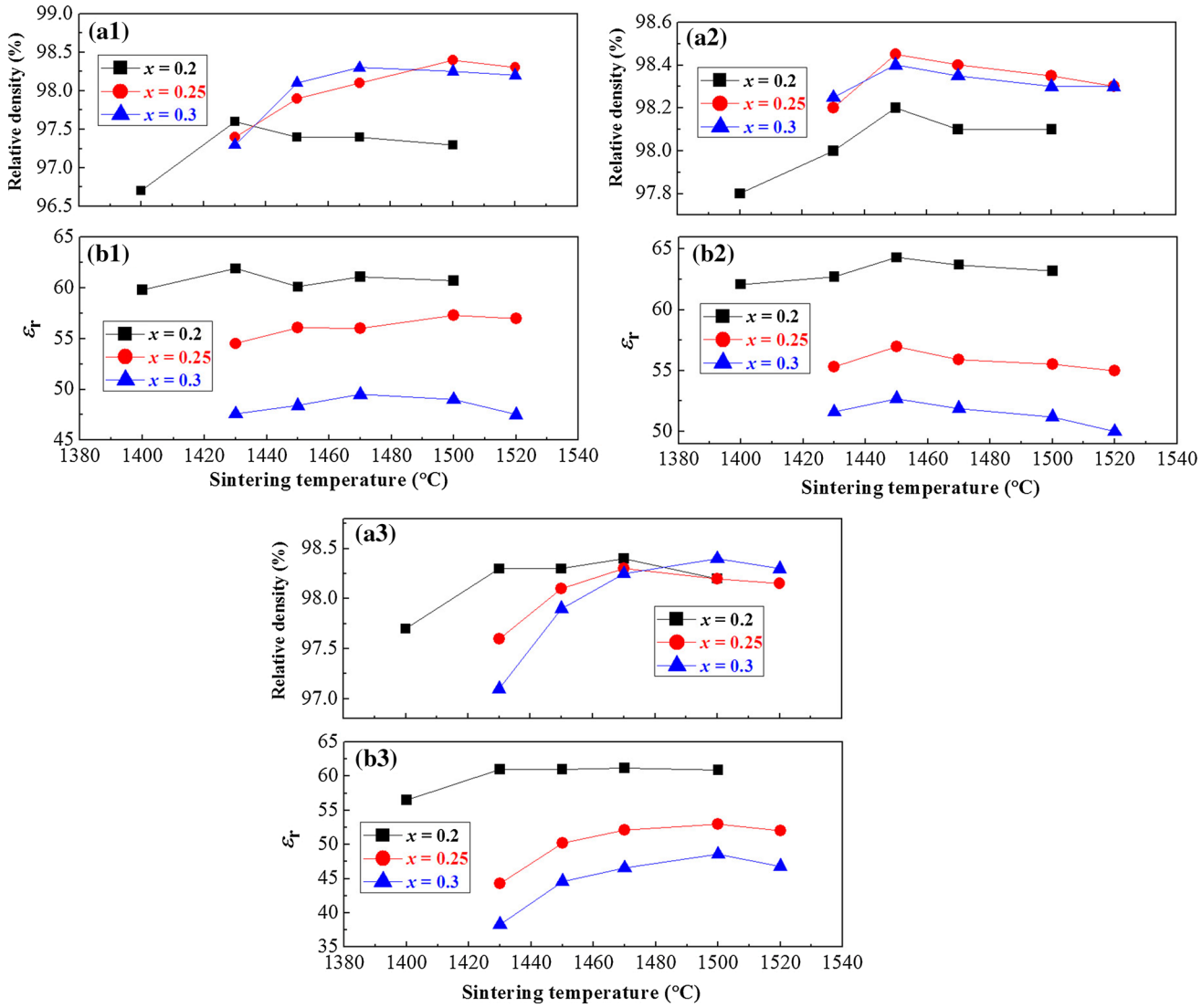

Fig. 5 Apparent density and ε_r of the **a1**, **b1** SNST-NAx, **a2**, **b2** SNST-PAx and **a3**, **b3** SNST-SAx ($0.2 \leq x \leq 0.3$) ceramics as a function of sintering temperature for 4 h

increase in x, the A-site bond valence increases while the B-site bond valence decreases for all the specimens, as shown in Table 2. It has been reported that the B-site bond valence of the perovskite structure is closely related to the temperature coefficient of the resonant frequency (τ_f). Kim and Yoon [34] suggest that the τ_f values of the $(1-x)CaTiO_3$–$xLi_{1/2}Sm_{1/2}TiO_3$ ($0.0 \leq x \leq 1.0$) ceramics decrease with an increasing of B-site bond valence, and Yang et al. [30] have reported the similar results in the $(Zn_{1-x}Mg_x)_3Nb_2O_8$ ($x = 0.02$–1.0) specimens. However, it has been shown the decrease of the τ_f values with decreasing of B-site bond valence in $(1-x)CaTiO_3$–$x(L_{i0.5}L_{a0.5})TiO_3$ ($0.2 \leq x \leq 0.8$) ceramics by Li et al. [20]. The common characteristic of these ceramic systems is that the τ_f values gradually shift to near zero or negative direction with the decrease in bond length between the B-site cation and oxygen. The same results are confirmed in the present work (Table 2). Thus we suggest that, according to the bond valence theory [33], the shorter the bond length is, the stronger the bond energy become. It also illustrates that the bond strength between B-site ion and oxygen will be stronger increasingly, which results in the decrease of the rattling effect in oxygen octahedra, and the τ_f values gradually reduce. Furthermore, τ_f values can be controlled by the substitution for the A-site ion. An increasing A-site bond valence gives rise to the increase in degree of oxygen octahedral tilting due to the change of ionic radius at the A-site, it also has some influence in a decreasing τ_f value [17]. To sum up, Fig. 7a–c shows the τ_f values of the SNST-NAx, SNST-PAx and SNST-SAx ($0.2 \leq x \leq 0.3$) ceramics as a function of A- and B-site bond valences. As increasing of the A-site bond valence, the τ_f values

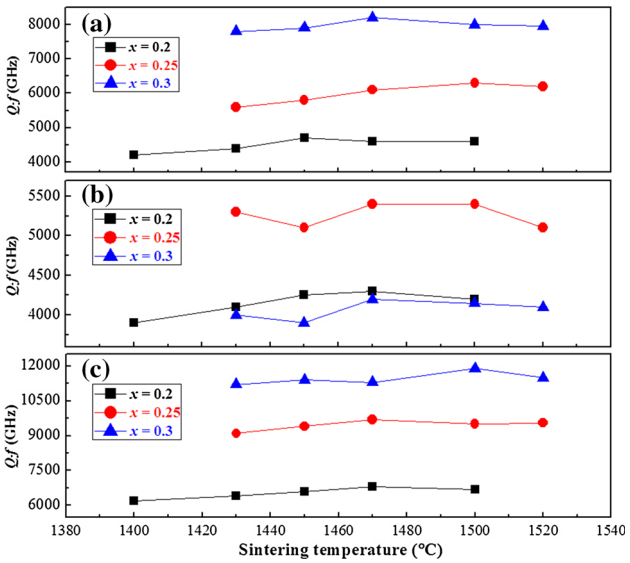

Fig. 6 The Room-temperature $Q{\cdot}f$ values with x for the **a** SNST-NAx, **b** SNST-PAx and **c** SNST-SAx ceramics as a function of sintering temperature for 4 h

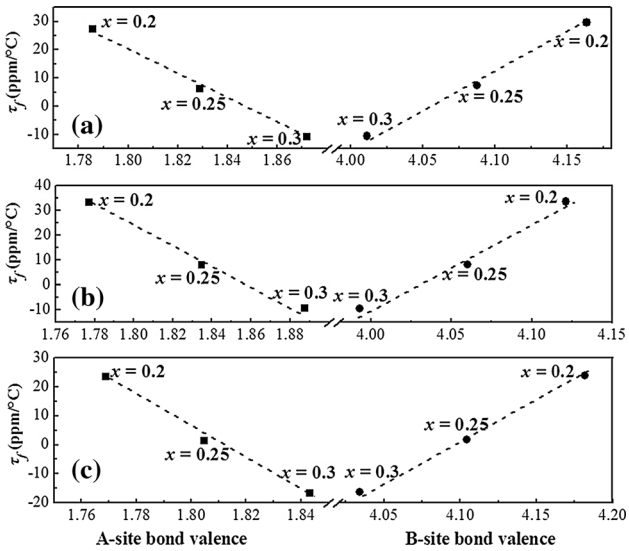

Fig. 7 τ_f values of the **a** SNST-NAx, **b** SNST-PAx and **c** SNST-SAx ($0.2 \leq x \leq 0.3$) ceramics as a function of A- and B-site bond valences

Table 2 Bond valence of the SNST-NAx, SNST-PAx and SNST-SAx ($0.2 \leq x \leq 0.3$) ceramics sintered at 1470 °C/4 h

Ln	x	R_{A-O} (Å)	d_{A-O} (Å)	v_{A-O}	V_{A-O}	b (Å)	R_{B-O} (Å)	d_{B-O} (Å)	v_{B-O}	V_{B-O}
Nd	0.2	2.0064	2.7113	0.1488	1.7856	0.37	1.7822	1.9175	0.6938	4.1628
	0.25	2.0133	2.7092	0.1524	1.8288	0.37	1.7739	1.9160	0.6811	4.0866
	0.3	2.0202	2.7076	0.1560	1.8721	0.37	1.7658	1.9149	0.6684	4.0104
Pr	0.2	2.0100	2.7165	0.1481	1.7772	0.37	1.7822	1.9212	0.6869	4.1214
	0.25	2.0178	2.7126	0.1529	1.8348	0.37	1.7739	1.9184	0.6767	4.0603
	0.3	2.0256	2.7099	0.1573	1.8876	0.37	1.7658	1.9165	0.6655	3.9930
Sm	0.2	2.0006	2.7089	0.1474	1.7688	0.37	1.7822	1.9158	0.6969	4.1818
	0.25	2.0061	2.7069	0.1504	1.8048	0.37	1.7739	1.9144	0.6840	4.1043
	0.3	2.0115	2.7045	0.1536	1.8432	0.37	1.7658	1.9127	0.6723	4.0340

decrease, while the τ_f values decrease with the decrease in B-site bond valence as well.

4 Conclusions

The microstructures and microwave dielectric properties of the SNSTx ($0.7 \leq x \leq 0.9$), SNST-NAx, SNST-PAx and SNST-SAx ($0.2 \leq x \leq 0.3$) ceramics have been investigated in this paper. The XRD results show that the $(1-x)Sr_{0.2}Na_{0.4}Sm_{0.4}TiO_3$–$xLnAlO_3$ (Ln = Nd, Pr and Sm) solid-solutions with the single orthorhombic perovskite phase can be formed in the componential range of $0.2 \leq x \leq 0.3$. The dielectric constant (ε_r) decreases with $LnAlO_3$ (Ln = Nd, Pr and Sm) content due to the smaller dielectric polarizability of $LnAlO_3$ than that of $(Sr_{0.2}Na_{0.4}Sm_{0.4})TiO_3$, and the ε_r is closely related to the compactness of ceramics as well. The quality factor ($Q{\cdot}f$) of all the specimens is strongly depended on grain sizes and grain boundaries. Moreover, the increasing A-site bond valence and the decreasing B-site bond valence lead to a decrease in the temperature coefficient of the resonant frequency (τ_f) in these ceramic specimens. The resultant dielectric properties have made the SNST-SA0.25 ($\varepsilon_r \sim 52.7$, $Q{\cdot}f \sim 9700$ GHz (at 4.33 GHz) and $\tau_f \sim 1.5$ ppm/°C) ceramics as very interesting materials for microwave communication and passive component applications.

Acknowledgments Financial supports of the National Natural Science Foundation of China (Grant No. 11464006), the Natural Science Foundation of Guangxi (Grant No. 2014GXNSFBA118254), the research fund of Guangxi Key Laboratory of Information Materials through 131018-Z, 131004-Z and Guangxi Experiment Center of Information Science through 20130115 are gratefully acknowledged by the authors.

References

1. C.F. Tseng, C.C. Huang, Microwave dielectric properties of $(1-x)Nd(Co_{1/2}Ti_{1/2})O_3$–$x(Ca_{0.8}Sr_{0.2})TiO_3$ composite ceramics. J. Mater. Sci. **47**, 3982–3988 (2012)
2. Changlai Yuan, Guohua Chen, Tao Yang et al., Microstructures and microwave dielectric properties of low-temperature fired $Ca_{0.8}Sr_{0.2}TiO_3$–$Li_{0.5}Sm_{0.5}TiO_3$ ceramics with Bi_2O_3–$2B_2O_3$ addition. J. Electron. Mater. (2014). doi:10.1007/s11664-014-3422-9
3. C.H. Hsun, S.H. Tsai, Dielectric characteristics of Sr substitution on $Ca_{0.4}Sm_{0.4}TiO_3$ ceramics at microwave frequency. Ceram. Int. **40**, 10111–10114 (2014)
4. I.M. Reaney, E.L. Colla, N. Setter, Dielectric and structural characteristics of Ba- and Sr-based complex perovskites as a function of tolerance factor. Jpn. J. Appl. Phys. **33**, 3984–3990 (1994)
5. H. Kagata, J. Kato, Dielelctric properties of Ca-based complex perovskite at microwave frequencies. Jpn. J. Appl. Phys. **33**, 5463–5465 (1994)
6. A. Manan, I. Qazi, A. Ullah, Preparation, characterization, and microwave dielectric properties of $Sr_2La_3Nb_{1-x}Ta_xTi_4O_{17}$ $(0 \leq x \leq 1)$ ceramics. J. Electron. Mater. **42**, 138–142 (2013)
7. J. Li, Y. Han, T. Qiu, C. Jin, Effect of bond valence on microwave dielectric properties of $(1-x)CaTiO_3$–$x(Li_{0.5}La_{0.5})TiO_3$ ceramics. J Mater. Res. Bull. **47**, 2375 (2012)
8. D.A. Abdel Aziz, I. Sterianou, I.M. Reaney, $(1-x)CaTiO_3$–$x(Li_{0.5}Nd_{0.5})TiO_3$ for ultra-small dielectrically loaded antennas. J. Mater. Sci. **44**, 6247 (2009)
9. B. Jancar, D. Suvorov, M. Valant, G. Drazic, Characterization of $CaTiO_3$–$NdAlO_3$ dielectric ceramics. J. Eur. Ceram. Soc. **23**, 1391–1400 (2003)
10. G.A. Ravi, F. Azough, R. Freer, Effect of Al_2O_3 on the structure and microwave dielectric properties of $Ca_{0.7}Ti_{0.7}La_{0.3}Al_{0.3}O_3$. J. Eur. Ceram. Soc. **27**, 2855–2859 (2007)
11. C.L. Huang, H.L. Chen, C.C. Wu, Improved high Q value of $CaTiO_3$–$Ca(Mg_{1/3}Nb_{2/3})O_3$ solid solution with near zero temperature coefficient of resonant frequency. Mater. Res. Bull. **36**, 1645–1652 (2001)
12. C.H. Hsu, H.A. Ho, Microwave dielectric in the $Sm(Co_{1/2}Ti_{1/2})O_3$–$CaTiO_3$ ceramic system with near-zero temperature coefficient with resonant frequency. Mater. Lett. **64**, 396–398 (2010)
13. E.A. Nenasheva, L.P. Mudroliubova, N.F. Kartenko, Microwave dielectric properties of ceramics based on $CaTiO_3$–$LnMO_3$ system (Ln–La, Nd; M-Al, Ga). J. Eur. Ceram. Soc. **23**, 2443–2448 (2003)
14. C.F. Tseng, C.L. Huang, W.R. Yang, Microwave dielectric properties of $xNd(Zn_{1/2}Ti_{1/2})O_3$–$(1-x)CaTiO_3$ ceramics. Mater. Lett. **61**, 4054–4057 (2007)
15. F. Liu, X.Y. Liu, C.L. Yuan et al., Crystal structure and dielectric properties of $(1-x)SrTiO_3$–$xCa_{0.4}Sm_{0.4}TiO_3$ ceramic system at microwave frequencies. Mater. Chem. Phys. **148**, 1083–1088 (2014)
16. F. Liu, C.L. Yuan, X.Y. Liu et al., Microstructures and dielectric properties of $(1-x)SrTiO_3$–$xCa_{0.61}Nd_{0.26}TiO_3$ ceramic system at microwave frequencies. J. Mater. Sci. Mater. Electron. (2014). doi:10.1007/s10854-014-2373-5
17. E.S. Kim, E.S. Chun, D.H. Kang, Effects of structural characteristics on microwave dielectric properties of $(1-x)Ca_{0.85}Nd_{0.1}TiO_3$–$xLnAlO_3$ (Ln = Sm, Er and Dy) ceramics. J. Eur. Ceram. Soc. **27**, 3005–3010 (2007)
18. H.J. Kim, S. Kucheiko, S.J. Yoon et al., Microwave dielectrics in the $(La_{1/2}Na_{1/2})TiO_3$–$Ca(Fe_{1/2}Nb_{1/2})O_3$ system. J. Am. Ceram. Soc. **80**, 1316–1318 (1997)
19. M.H. Kim, S. Nahm, C.H. Choi et al., Dielectric properties of $(1-x)NdGaO_3$–$xCaTiO_3$ solid solution at microwave frequencies. Jpn. J. Appl. Phys. **41**, 717–721 (2002)
20. J.M. Li, Y.X. Han, T. Qiu et al., Effect of bond valence on microwave dielectric properties of $(1-x)CaTiO_3$–$x(Li_{0.5}La_{0.5})TiO_3$ ceramics. J Mater. Res. Bull. **47**, 2375 (2012)
21. P.L. Wise, I.M. Reaney, W.E. Lee et al., Structure microwave property relations in $(Sr_xCa_{1-x})_{n+1}Ti_nO_{3n+1}$. J. Eur. Ceram. Soc. **21**, 1723–1726 (2001)
22. Y. Konishi, Novel dielectric wave guide components-microwave applications of new ceramic materials. Proc. IEEE **79**, 726–740 (1991)
23. N. Ichinose, N. Chida, Microwave dielectric properties of $(Li_{1/2}Nd_{1/2})TiO_3$–$(Na_{1/2}Ln_{1/2})TiO_3$ (Ln = La, Nd, Sm) ceramic system. Proc. IEEE Int. Symp. **196**, 513–514 (1998)
24. C. Zuccaro, W. Winter, N. Klein et al., Microwave absorption in single crystals of lanthanum aluminate. J. Appl. Phys. **82**, 5695–5704 (1997)
25. D. Mateika, H. Kohler, H. Landern et al., Mixed perovskite substrate for high Tc superconductors. J. Cryst. Growth **109**, 447–456 (1991)
26. J. Krupka, K. Derzakowski, B. Riddle et al., A dielectric resonator for measurements of complex permittivity of low loss materials as a function of temperature. Meas. Sci. Technol. **9**, 1751–1756 (1998)
27. T. Nishikawa, K. Wakino, H. Tamura et al., Precise measurement method for temperature coefficient of microwave dielectric resonator material. IEEE. MTT-S. Int. Microwave. Symp. Dig. **3**, 277–280 (1987)
28. R.D. Shannon, Revised effective ionic radii and systematic studies of interatomic distances in halides and chalcogenides. Acta. Cryst. A. **32**, 751–767 (1976)
29. D.M. Iddle, A.J. Bell, A.J. Moulson, Relationships between dopants, microstructure and the microwave dielectric properties of ZrO_2–TiO_2–SnO_2 ceramic. J. Mater. Sci. **27**, 6303 (1992)
30. W.R. Yang, C.C. Pan, C.L. Huang, Influence of Mg substitutions for Zn on the phase relation and microwave dielectric properties of $(Zn_{1-x}Mg_x)_3Nb_2O_8$ $(x = 0.02–1.0)$ system. J. Alloys Comp. **581**, 257–262 (2013)
31. R.D. Shannon, Dielectric polarizabilities of ions in oxides and fluorides. J. Appl. Phys. **73**, 348–366 (1993)
32. E.S. Kim, B.S. Chun, D.W. Yoo et al., Microwave dielectric properties of $(1-x)(Ca_{0.7}Nd_{0.2})TiO_3$–$x(Li_{0.5}Nd_{0.5})TiO_3$ ceramics. Mater. Sci. Eng. B **99**, 247–251 (2003)
33. N.E. Brese, M. O'Keeffe, Bond-valence parameters for solids. Acta. Cryst. **B47**, 192–197 (1991)
34. E.S. Kim, K.H. Yoon, Microwave dielectric properties of $(1-x)CaTiO_3$–$xLi_{1/2}Sm_{1/2}TiO_3$ ceramics. J. Eur. Ceram. Soc. **23**, 2397–2401 (2003)